Materials Advances

ROYAL SOCIETY OF CHEMISTRY

PAPER

View Article Online
View Journal | View Issue

Cite this: *Mater. Adv.*, 2023, 4, 2292

Hydrothermal synthesis of zeolites using silica extracted from tropical volcanic ash

Stephen O. Otieno,[a] Fredrick O. Kengara,[b] Chrispin O. Kowenje*[a] and Robert Mokaya *[c]

Received 9th February 2023, Accepted 6th April 2023

DOI: 10.1039/d3ma00065f

rsc.li/materials-advances

This study addresses the reliance on costly aluminosilicate sources for the synthesis of zeolites by exploring the use of silica extracted from tropical volcanic ash. The volcanic ash contained CaO, in the form of calcite polymorph of $CaCO_3$, and silica at 47.09 wt% and 18.38 wt%, respectively. High purity silica was obtained by simply washing the volcanic ash with HCl to remove the calcite, and was then used, with additional commercial aluminate, in the synthesis of varieties of zeolites *via* the fusion method. The type of zeolite prepared, Na–X, Na–P or hydroxysodalite (Na-HS), was determined by the $SiO_2 : Al_2O_3 : Na_2O : H_2O$ molar ratios and in particular the amount of SiO_2 and Na_2O. The Na–X product had the highest surface area (766 $m^2\ g^{-1}$), micropore surface area (644 $m^2\ g^{-1}$) and pore volume (0.26 $m^3\ g^{-1}$), and these textural values were comparable to those of commercial molecular sieve 13X. This work demonstrates that (i) high purity silica can be obtained from abundant and inexpensive volcanic ash by simple acid treatment, and (ii) the silica can be used in the production of high purity zeolites, whose quality is dependent on the hydrogel composition.

1. Introduction

Zeolites are porous inorganic materials consisting of tetrahedra that are linked *via* oxygen bridges. Natural zeolites occur as cavity fillings in mafic rocks and as alteration products of volcanic glass in sedimentary rocks.[1] Their formation is as a result of the reaction between volcanic ash components and underground basic water at temperatures below 200 °C. Although natural zeolites are abundant,[2] synthetic zeolites are more commonly used because of their high purity, sorption capacity, ion exchange properties and catalytic activity.[3] Hydrothermal synthesis, involving the treatment of aluminates and silicates in alkaline media at elevated pressures and low to moderate temperatures, is the most favoured method for the synthesis of zeolites because it mimics the natural conditions under which zeolite minerals are formed in the earth's crust.[2] Alkaline media helps in the dissolution and gelatinization of the aluminosilicate components before the crystallization step. The large number of ways *via* which silica and alumina tetrahedral ions can be linked during the gelatinization and crystallization stages allow for the formation of a variety of zeolite types but with uniformly sized pores for any specific zeolite product.

Current production of zeolites utilizes costly commercial sources of aluminates and silicates.[4] In order to lower the cost of production, on-going research seeks to synthesize zeolites from alternative low cost natural materials. Although alternative materials such as industrial[5] and agricultural waste,[6] coal fly ash,[7] rice husk,[8,9] and kaolin clay[10] among others, have been used as possible precursors for the synthesis of zeolites, sustainable preparation routes would best focus on natural resources that are rich in aluminates and silicates such as clay and volcanic ash materials, both of which are abundant in the earth's crust. However, while the synthesis of zeolites from clay minerals has been extensively studied,[10–15] reports on the use of volcanic ash as a raw material are limited. This may be due to the fact that volcanic ash materials are heterogeneous in composition meaning that the nature of volcanic ash varies according to its source.[16–21] The conversion of volcanic ash to zeolites is therefore a challenge due to these variations. Nonetheless, volcanic ash is rich in aluminates and silicates, and its exploitation in the zeolite industry is worth exploring.

In order to overcome the challenges caused by the heterogeneous nature of natural materials in their use for the synthesis of zeolites, studies have evolved ranging from the reaction of raw aluminosilicates with basic solutions,[22–24] to their pre-treatment by fusion with alkalis before hydrothermal synthesis.[13,14,25] In this study, various zeolites were synthesized using volcanic ash *via* the fusion method. The effect of the amount of various oxides in the synthesis hydrogels was also investigated by varying the $SiO_2 : Al_2O_3 : Na_2O : H_2O$ molar ratios.

---

[a] Department of Chemistry, Maseno University, P. O. Box, 333-40105, Maseno, Kenya. E-mail: ckowenje@maseno.ac.ke
[b] School of Pure and Applied Sciences, Bomet University College, P. O. Box 701-20400, Bomet, Kenya
[c] School of Chemistry, University of Nottingham, University Park, Nottingham NG7 2RD, UK. E-mail: r.mokaya@nottingham.ac.uk

2. Materials and methods

2.1 Materials

All chemicals and reagents used in this study were of analytical grade unless otherwise specified. The tropical volcanic ash (TVA) was obtained from the slopes of Mt. Eburu Volcano in Nakuru County, Kenya (0°34′27.2″S 36°15′43.9″E). Molecular sieve 4A and molecular sieve 13X (4–8 mesh) were obtained from Alfa Aesar Chemicals – UK. Sodium hydroxide (NaOH, 99% purity), and hydrochloric acid (HCl, 37% purity) were obtained from Fisher Scientific – UK. Sodium aluminate powder ($NaAlO_2$) was obtained from MP Biomedicals, LLC – USA. Lithium tetraborate ($\geq$99.9% trace metal basis) was from Honeywell – UK. The 28 component ICP-OES standard solution containing 100 ml L^{-1} of each metal ion component in 5% HNO_3 and the silicon standard solution (100 ml L^{-1}) in 5% HNO_3 were obtained from Fisher Scientific – UK. Deionized water was prepared using an Elga PURELAB Option 4463 water deionizer.

2.2 Extraction of volcanic silica

The raw volcanic ash (r-TVA) was extracted from the volcanic tuffs by carefully extracting the white soft solids from the tuffs. The extraction process is shown in Fig. 1. The extracted material was ground to powder and then passed over a magnetic surface to remove magnetic components. The resulting powder was washed several times with deionized water at room temperature before drying in an oven at 100 °C for 24 h. The dried powder was further purified by washing in HCl by stirring 100 g of the dried powder in 600 ml of 2.74 M HCl for 24 h at 600 rpm at room temperature. The acid-washed material was then washed several times with deionized water to pH *ca.* 7 before drying in the oven at 100 °C for 24 h to obtain purified volcanic ash (p-TVA).

2.3 Hydrothermal crystallization of zeolites

Zeolites were synthesized hydrothermally using purified volcanic ash (p-TVA) as a natural source of high purity silica, and commercial sodium aluminate as a source of alumina. The procedure used for pre-treatment of the starting materials involved wet mixing followed by dry fusion as previously reported.[14] In brief, 3.07 g of sodium hydroxide was added to a mixture of 3.13 g of sodium aluminate and 4.69 g of p-TVA. 3.5 ml of water was then added to dissolve the NaOH and aid in achieving a homogenous mixture of the materials in the form of a paste. The resulting paste was dried in an oven at 100 °C for 48 h before fusing at 750 °C for 8 h. 6.83 g of the resulting fused material (F-TVA) was then dissolved in 50.6 ml of water followed by stirring at 600 rpm for 4 h to dissolve the components and achieve a homogeneous hydrogel. The resulting hydrogel was aged for 24 h at room temperature and ambient pressure under static conditions before being subjected to hydrothermal crystallization at 100 °C for 48 h. The synthesized zeolites were washed with deionized water to pH $<$ 8 followed by drying at 100 °C for 24 h in the oven. The dried zeolites were kept in caped vials prior to further characterization. The effects of the amount of SiO_2, Al_2O_3, Na_2O and H_2O in the synthesis hydrogel were investigated by varying the $SiO_2 : Al_2O_3 : Na_2O : H_2O$ molar ratios as shown in Table 1.

Table 1 Variations in the synthesis hydrogel composition

	Hydrogel composition
Product code	$SiO_2 : Al_2O_3 : Na_2O : H_2O$
SZ1-VA-48h	2.4 : 1.0 : 3.0 : 120.6
SZ2-VA-48h	4.1 : 1.0 : 3.0 : 221.1
SZ3-VA-48h	2.0 : 1.0 : 1.9 : 107.0

2.4 Characterization

The chemical composition of the volcanic ash and zeolites was determined using a PerkinElmer Inductively Coupled Plasma Optical Emission Spectroscopy (ICP-OES) Optima 2000 DV. The samples and reference standards were prepared and analyzed as previously reported.[14,15] The presence of functional groups was monitored by infrared spectroscopy using a Bruker Alpha Attenuated Total Reflectance – Fourier Transform Infrared (ATR-FTIR) spectrometer. 1 mg of powder sample was placed on a diamond crystal, and the anvil lowered to enforce contact of the sample with the crystal. Powder XRD patterns were obtained in continuous mode using a PANalytical X-Pert Pro X-ray powder diffractometer employing Cu-Kα radiation. X-rays were generated from the Cu anode at 40 kV and a current of 40 mA. Diffraction patterns were recorded at room temperature over the 2θ range from 5° to 50° in steps of 0.026°. Zeolite phases were identified by comparison with those of commercial zeolites and the reference XRD patterns in the zeolite database from the International Zeolite Association.[26] The surface

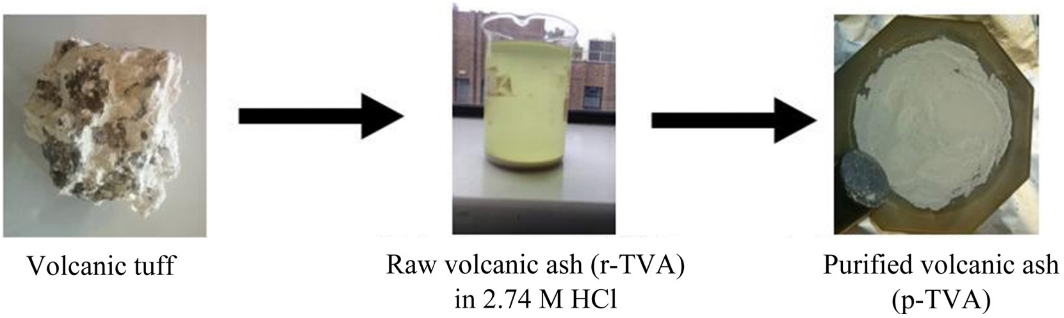

Fig. 1 Extraction of tropical volcanic ash material from volcanic tuff.

Table 2 Chemical composition of raw volcanic ash (r-TVA), purified volcanic ash (p-TVA) and the zeolite products

	Percent oxide (wt%)									
Sample	Al_2O_3	SiO_2	Na_2O	TiO_2	Fe_2O_3	K_2O	CaO	CuO	SiO_2/Al_2O_3	LOI
r-TVA	0.36	18.38	0.72	0.15	0.03	0.03	47.09	0.23	88.23	33
p-TVA	0.24	98.92	0.57	0.02	0.04	0.04	—	0.16	707.67	
SZ1-VA-48h	30.27	46.71	22.63	0.01	0.07	0.13	—	0.17	2.62	
SZ2-VA-48h	29.84	46.44	23.05	0.02	0.23	0.27	—	0.14	2.64	
SZ3-VA-48h	34.11	40.65	24.48	0.52	0.24	—	—	—	2.02	

morphology of the samples was explored *via* scanning electron microscopy (SEM) using a Field Electron and Ion (FEI) Quanta 200 3D Dual Beam focused ion beam (FIB) microscope. The samples were coated with palladium prior to analysis. Thermogravimetric analysis (TGA) was performed using a TA Instruments SDT Q600 thermal analyzer. 10 mg of the sample was heated to 1000 °C at heating ramp rate of 10 °C min^{-1} under flowing air (100 mL min^{-1}). The textural properties of the zeolites were obtained using a Micromeritics 3FLEX sorptometer employing N_2 gas as a sorbate at −196 °C. Approximately 100 mg of the sample was outgassed under vacuum at 300 °C for 16 h before analysis. The surface area was calculated using the BET method and the pore volume was obtained from the N_2 uptake at close to saturation pressure ($P/P_0 \sim 0.99$). The micropore surface area, external surface area and micropore volume were determined from *t*-plot analysis. The Horvath–Kawazoe model, assuming spherical pore geometry due to the three-dimensional pore structure of zeolites, was used to model the pore size distribution of the zeolites.

3. Results and discussion

3.1 Characterization of volcanic ash

The chemical composition of the raw and purified volcanic ash is shown in Table 2. The raw volcanic ash (r-TVA) has two main ingredients, namely, CaO and SiO_2 at 47.09 wt% and 18.38 wt%, respectively. A total of 33% weight loss was observed as a loss on ignition (LOI) for the raw volcanic ash. The oxides of Al, Na, Ti, Fe, K and Cu were detected but at trace levels. Although our sample showed trace amounts of Al_2O_3, other studies have reported higher alumina content in volcanic ashes.[16–20] The CaO was removed on purification, *i.e.*, washing with 2.74 M HCl, resulting in purified volcanic ash (p-TVA) with 99% SiO_2, which was subsequently used as a high purity silica source for zeolite synthesis.

The surface morphology of the raw and purified volcanic ash is illustrated in the SEM images in Fig. 2. The raw volcanic ash (Fig. 2a) appears to be a porous material with rough surface topology. An apparently less porous material (Fig. 2b), the high purity silica, was obtained after washing with acid. Regarding functional groups, the FTIR bands (Fig. 2c) at 449, 794 and 1062 cm^{-1} are due to Si–O symmetric bending, and in plane or out of plane stretching vibrations of the amorphous SiO_2, respectively. The band at *ca.* 779 cm^{-1} is due to quartz phase Si–O. The bands at *ca.* 712, 872, and 1412 cm^{-1} in the r-TVA spectrum are characteristic of calcite polymorph of calcium carbonate mineral and correspond to the in-plane bending (v_4), out of plane bending (v_2) and symmetric stretching (v_3) modes of the calcite carbonate ($-CO_3$) group.[27] Other calcium carbonate bands appear at *ca.* 1796, 2507 and 3695 cm^{-1}.[27,28] The bands at 667 and 1015 cm^{-1} have previously been reported for poorly ordered amorphous $CaCO_3$ phases.[29] The bands due to amorphous SiO_2 in the r-TVA spectrum were masked by the intense calcite bands. All the calcite bands were eliminated on purification of the volcanic ash after washing with HCl. The FTIR spectra of the calcined purified volcanic ash (p-TVA-750C) matches that of commercial fumed silica (Fig. 2c).

The XRD patterns of the raw and purified volcanic ashes are shown in Fig. 2d. The peaks at 2θ of 23.2°, 29.5°, 31.6°, 17.4°, 39.5°, 43.3°, 47.3°, 47.7° and 48.7° in the raw volcanic ash pattern have previously been observed and ascribed to calcite polymorph of $CaCO_3$.[30] All the calcite peaks were absent in the pattern of the purified volcanic ash. An amorphous silica phase, with a broad peak at 2θ of between 17° and 34°, results from the purification process. The other sharp peaks in the pattern of the purified ash, at 2θ of 21.1°, 26.8°, 36.7°, 39.6°, 40.3°, 42.6° and 46.0°, arise from quartz phase.[26] The amorphous silica and quartz peaks were, however, suppressed in the XRD pattern of the r-TVA by the intense calcite peaks. The observations made in the XRD patterns are therefore in good agreement with those from the FTIR spectra, SEM images and elemental composition.

Fig. 2(e and f) shows the TGA, DTA and DSC curves for the raw and purified volcanic ash materials. The raw volcanic ash (Fig. 2e) appears to be highly thermally stable with only 1% weight loss up to 620 °C due to removal of absorbed water. This was then followed by an endothermic weight loss of 33% between 620 and 815 °C, with the point of maximum loss appearing at 790 °C, due to the decomposition of calcite to CaO accompanied by loss of CO_2.[28] The 33% weight loss is in agreement with the observed loss on ignition (LOI) for the raw volcanic ash (r-TVA) according to the chemical composition in Table 2. On the other hand, a total of 3% weight loss, due to absorbed water, was recorded for the purified volcanic ash in Fig. 2f.

3.2 Characterization of zeolite products

The chemical composition of the zeolite products is shown in Table 2. It should be noted that the difference between SZ1-VA-48h and SZ2-VA-48h hydrogels was the amount of SiO_2, with the SZ2-VA-48h hydrogel having greater amounts (Table 1). On the other hand, the difference between SZ1-VA-48h and SZ3-VA-48h was the amount of Na_2O used, with the SZ1-VA-48h hydrogel

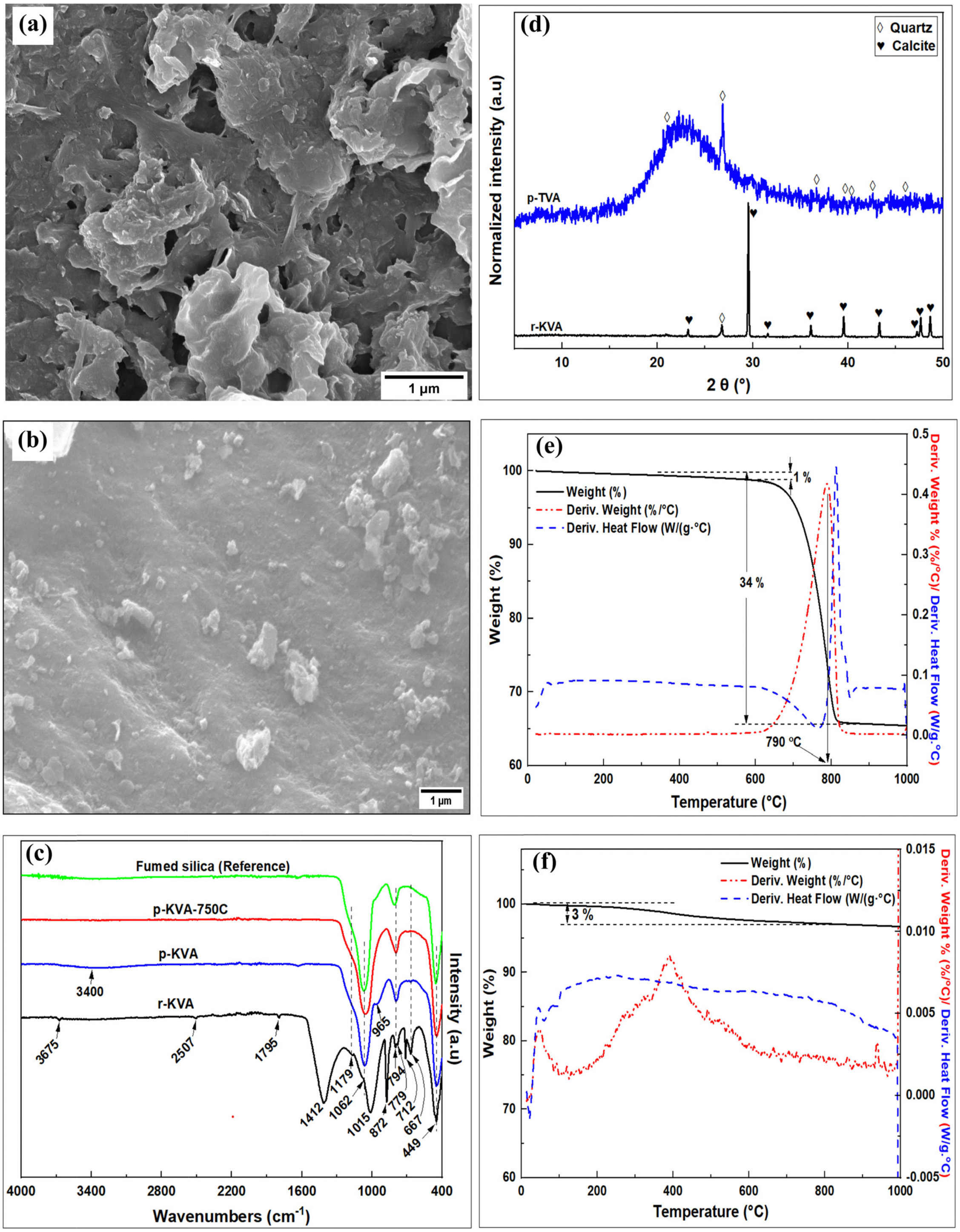

Fig. 2 Characterization of raw and purified volcanic ash materials; (a and b) SEM images; (c) FTIR spectra; (d) XRD patterns; and (e and f) TGA curves.

having greater amounts. The differences in amounts of SiO_2 and Na_2O in the hydrogels were, however, not reflected in the Si and Na content of the zeolite products. For example, in spite of the large differences in SiO_2 content in their hydrogels, SZ1-VA-48h and SZ2-VA-48h had similar SiO_2 content at 46 wt%. Similarly, the Na_2O content of SZ1-VA-48h and SZ3-VA-48h was the same at *ca.* 24%. The elemental composition of the resulting zeolite products is therefore not dependent on the synthesis hydrogel composition but rather on the nature of the resulting zeolite framework type.

3.2.1 Identification of zeolite products. The transformation of fused volcanic ash (F-TVA) to zeolite products was monitored using FTIR spectroscopy (Fig. 3). The FTIR spectra, especially in the finger print region of 400–1000 cm^{-1}, show

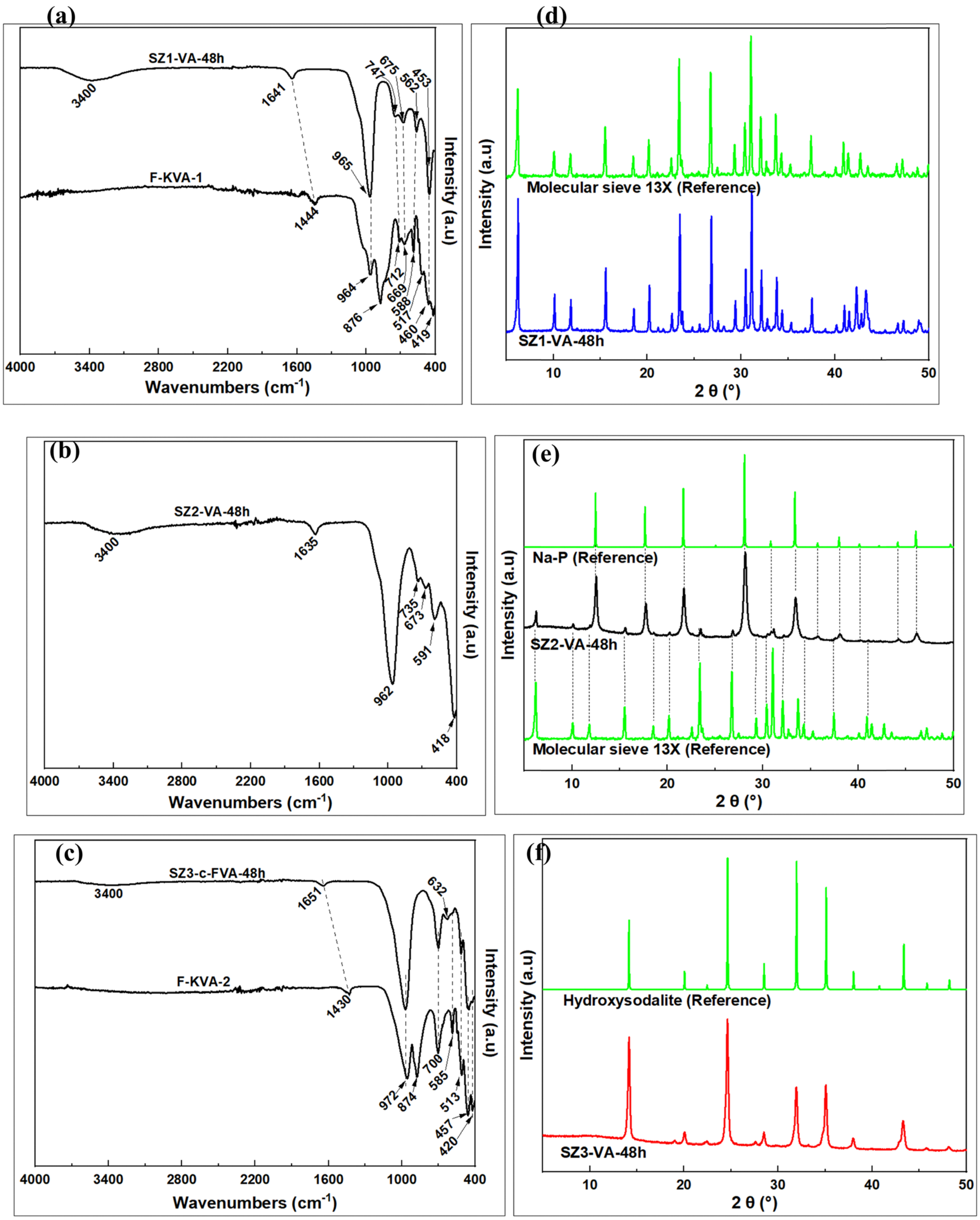

Fig. 3 Characterization of the products; FTIR spectra of the fused volcanic ash (F-TVA) and the zeolite products (a–c), and XRD patterns of the zeolite products (d–f).

that different zeolite products were obtained depending on the composition of the hydrogel. However, the spectral bands for both fused-volcanic ashes (*i.e.*, F-TVA-1 and F-TVA-2) show some similarities with the spectra of corresponding products. This suggests the presence of pre-formed zeolite seeds, which is consistent with previous reports.[13,14] The spectral bands of the products and their assignments are shown in Table 3. All the IR bands for SZ1-VA-48h are characteristic of zeolite Na–X.[31] Similar absorption bands were observed for the SZ2-VA-48h product, but the bands at 418, 735 and 1635 cm^{-1} were at lower wavenumbers. On the other hand, the adsorption bands at 420 cm^{-1}, 457 cm^{-1}, 700 cm^{-1}, 972 cm^{-1} in SZ3-VA-48h are characteristics of hydroxysodalite (Na-HS).[32,33]

The XRD patterns in Fig. 3(d–f) show some interesting variations. The peaks at 2θ of 6.15°, 10.06°, 15.51°, 20.11°, 23.34°, 26.67°, 30.35°, 30.98°, 32.06° and 33.61° for SZ1-VA-48h

Table 3 Spectral bands of the zeolite products, namely, A = SZ1-VA-48h, B = F-TVA-1, C = SZ2-VA-48h, D = SZ3-VA-48h, E = F-TVA-2

Spectral bands (cm^{-1})						
A	B	C	D	E	Assignment	Ref.
	419	418		420	Single four-membered ring (S4R) of the sodalite – adsorption at 428 cm^{-1}	
443	460		457	457	Symmetric bending vibrations of T–O tetrahedral	34
	517		513	513	[a]	
562	588	591	585	585	Symmetric stretching vibrations associated with the six-member rings (D6R) of the faujasite structure	
					Double four-membered ring (D4R)	31
675	669	673	632		Internal symmetric stretching of zeolitic T–O tetrahedral	34
747	712	735	700	700	External symmetric stretching vibration of T–O–T	
	876			874	[a]	
965	964	962	972	972	Internal asymmetric stretching vibrations of zeolitic T–O–T tetrahedral	34
1641	1444	1635	1651	1430	Bending vibration of adsorbed water	35
3400		3400	3400		Stretching vibration of adsorbed water	35

[a] Unidentified bands.

in Fig. 3d are characteristic of zeolite Na–X,[26] and indeed match those expected for molecular sieve 13X. The XRD pattern of SZ2-VA-48h (Fig. 3e) suggests the presence of a mixture of zeolites. The intense peaks at 2θ of 12.5°, 17.6°, 21.7°, 28.1°, 33.4°, 38.0° and 46.0° are characteristic of zeolite Na–P,[26] while the low intensity peaks at 2θ of 6.2°, 10.0°, 15.5°, 18.51°, 20.2°, 23.4°, 26.8°, 29.3°, 3.4° and 32.1°, are typical of zeolite Na–X[26] and match those of the molecular sieve 13X. On the other hand, all the XRD peaks for SZ3-VA-48h (Fig. 3f) at 2θ of 14.2°, 20.0°, 22.5°, 24.6°, 28.5°, 32.0°, 35.1°, 38.0°, 40.8°, 43.4°, 45.8° and 48.2° are characteristic of hydroxysodalite.[26]

The SEM image of SZ1-VA-48h (Fig. 4a) shows octahedral crystals of varying size that are similar to those previously reported for zeolite Na–X.[13,14] On the other hand, the SEM image of SZ3-VA-48h (Fig. 4b) consists of irregular shaped cubic-like and spherical particles of size ranging between 50 and 300 nm. These irregular cubic and spherical particles have previously been observed for hydroxysodalite.[33] The SEM image of SZ2-VA-48h (Fig. 4c) shows spheres as large as 5 μm in diameter and with rugged surface morphology. The spheres are a result of aggregation of prismatic particles with sharp edges as shown in Fig. 4d (the magnified image of the surface of the spherical aggregates in Fig. 4c). Such aggregates and morphologies are characteristics of zeolite Na–P, and are consistent with other reports.[36,37] The few clusters of octahedral particles among the Na–P spheres and on the surface of the spheres belong to Na–X. The small number of Na–X particles in the SEM image is in agreement with the low intensity of Na–X peaks (in comparison to those of Na–P) in the relevant XRD pattern (Fig. 3e).

The foregoing discussion indicates that the zeolite framework type formed depended on the SiO_2 and Na_2O content of the hydrogels. Low amounts of SiO_2 resulted in either high purity Na–X (SZ1-VA-48h) or hydroxysodalite (SZ3-VA-48h), while high amounts generated a mixture of Na–X and Na–P zeolites (SZ2-VA-48h). For the low SiO_2 hydrogels, low Na_2O content resulted in a high purity hydroxysodalite phase (SZ3-VA-48h) while high Na_2O content resulted in high purity Na–X (SZ1-VA-48h). The oxide composition of the products is, however, independent of the hydrogel composition as observed in the chemical composition in Table 2.

3.2.2 Thermogravimetric analysis of the zeolite products.

The TGA, DTA and DSC curves of the zeolite products are shown in Fig. 4(e–g). The TGA curves of SZ1-VA-48h and SZ3-VA-48h (Fig. 4e and g) show that endothermic desorption of water occurred in a single step between 25 and 400 °C accompanied with 23% and 7.5% weight loss, respectively. The single step weight loss corresponds to the desorption of water from uniform pores of Na–X and hydroxysodalite zeolites. The desorption was, however, a slow process for SZ3-VA-48h (Na-HS) when compared to SZ1-VA-48h (Na–X). This is because the mass transfer of the water molecules is hindered by the small pores of Na-HS. On other hand, 18% weight loss occurred in multiple steps between 25 and 800 °C for SZ2-VA-48h (Fig. 4f). The multiple steps correspond to desorption of water from different pore sizes of the Na–X and Na–P zeolite mixture.

3.2.3 Surface area and porosity of zeolite products.

The sorption isotherms and pore size distribution curves of the products are shown in Fig. 5 and the textural properties are summarised in Table 4. All zeolite products show type I isotherm typical of microporous materials.[38] The SZ1-VA-48h (Na–X) product has high surface area, micropore surface area and pore volume of 766 $m^2\ g^{-1}$, 644 $m^2\ g^{-1}$ and 0.26 $cm^3\ g^{-1}$, respectively. These textural properties are comparable to those of the commercial molecular sieve 13X (*i.e.*, 772 $m^2\ g^{-1}$, 723 $m^2\ g^{-1}$ and 0.30 $cm^3\ g^{-1}$). On the other hand, the SZ2-VA-48h product had very low surface area and pore volume of 12 $m^2\ g^{-1}$ and 0.04 $cm^3\ g^{-1}$, respectively. Regarding the nature of SZ2-VA-48h, the intense peaks ascribable to Na–P zeolite in the XRD pattern (Fig. 3e), and the large number of crystallite particles in the SEM images (Fig. 4c and d), are a clear indication that Na–P zeolite occurs in greater amounts than Na–X zeolite. In such a scenario, the small pores (2.9 Å)[37] of Na–P would hinder N_2 gas sorption, which would explain the low porosity and textural properties observed. Similarly, the low surface area and micropore volume recorded for SZ3-VA-48h is due to the small pore openings (4.2 Å) of hydroxysodalite,[39] which also hinder N_2 sorption. Pore size of 9.1 Å and 7.7 Å was observed for Na–X (in SZ1-VA-48h) and Na-HS (in SZ3-VA-48h), respectively.

4. Conclusions

Raw tropical volcanic ash (r-TVA) is mainly composed of silica (SiO_2) and calcite ($CaCO_3$) and is thermally stable up to 620 °C,

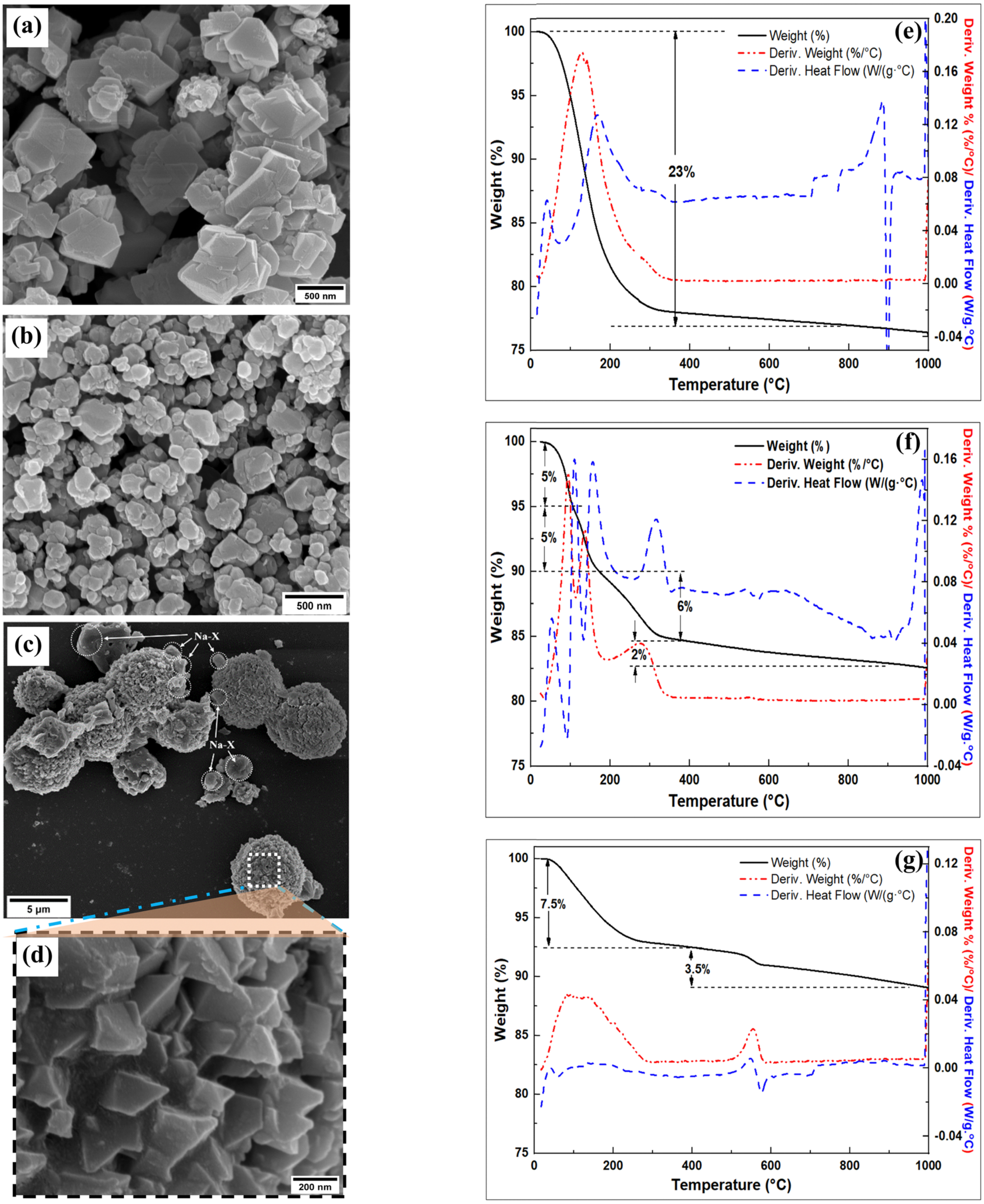

Fig. 4 Characterization of the products; SEM images (a) SZ1-VA-48h; (b) SZ3-VA-48h; (c and d) SZ2-VA-48h), and TGA analysis (e) SZ1-VA-48h; (f) SZ2-VA-48h; (g) SZ3-VA-48h).

with the calcite decomposing to CaO between 620 and 815 °C. The r-TVA may be used as a source of high purity silica once the calcite phase is removed by washing in HCl. A variety of high quality and high purity zeolite products, whose properties depend on the SiO_2 and Na_2O content of their synthesis hydrogels, can be obtained from the volcanic ash *via* fusion and hydrothermal methods. Low silica hydrogels resulted in either high purity Na–X or hydroxysodalite, while high SiO_2 amounts resulted in a mixture of Na–X and Na–P zeolites. For the low SiO_2 hydrogels, low Na_2O content resulted in high purity hydroxysodalite while high Na_2O content resulted in high purity Na–X zeolite. The oxide composition of the products is, however, independent of the synthesis hydrogel composition. Na–X (SZ1-VA-48h) had the highest surface area (766 $m^2\ g^{-1}$), micropore surface area (644 $m^2\ g^{-1}$) and pore volume (0.26 $cm^3\ g^{-1}$), which are comparable to those of commercial molecular sieve 13X.

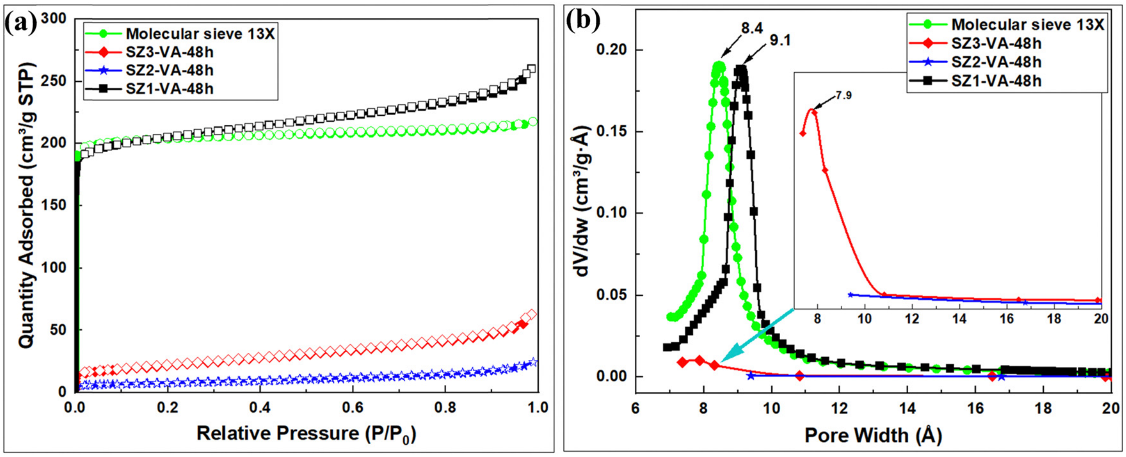

Fig. 5 Porosity analysis; (a) N_2 sorption isotherms, and (b) Horvath–Kawazoe pore size distribution curves of synthesized zeolites.

Table 4 Textural properties of synthesized zeolites

Sample	Surface area (m^2 g^{-1})	Micropore surface area (m^2 g^{-1})	External surface area (m^2 g^{-1})	Pore volume (cm^3 g^{-1})	Micropore volume (cm^3 g^{-1})	Pore size (Å)
SZ1-VA-48h	766	644	122	0.40	0.26	9.1
SZ2-VA-48h	12	—	18	0.04	—	—
SZ3-VA-48h	75	5	71	0.10	0.003	7.7
Molecular sieve 13X	772	727	46	0.34	0.30	8.7

Conflicts of interest

There are no conflicts to declare.

Acknowledgements

This work was supported by the Royal Society (ACBI programme grant number AQ150029). We thank the School of Chemistry, University of Nottingham for assistance with various aspects of this work. RM thanks the Engineering and Physical Sciences Research Council (EPSRC) for an equipment grant and Royal Society for a Royal Society Wolfson Research Merit Award.

References

1 D. Alderton, in *Encyclopedia of Geology*, ed. D. Alderton and S. A. Elias, Academic Press, Oxford, 2nd edn, 2021, pp. 313–325.
2 M. Król, *Crystals*, 2020, **10**, 622.
3 V. C. De Souza, J. Villarroel-Rocha, M. J. G. De Araújo, K. Sapag and S. B. C. Pergher, *Minerals*, 2018, **8**, 595.
4 S. Mukherjee, S. Barman and G. Halder, *Groundwater Sustainable Dev.*, 2018, **7**, 39–47.
5 M. Yoldi, E. G. Fuentes-Ordoñez, S. A. Korili and A. Gil, *Microporous Mesoporous Mater.*, 2019, **287**, 183–191.
6 S. Bohra, D. Kundu and M. K. Naskar, *Ceram. Int.*, 2014, **40**, 1229–1234.
7 D. Längauer, V. Čablík, S. Hredzák, A. Zubrik, M. Matik and Z. Danková, *Materials*, 2021, **14**, 1267.
8 R. M. Mohamed, I. A. Mkhalid and M. A. Barakat, *Arabian J. Chem.*, 2015, **8**, 48–53.
9 C. G. Flores, H. Schneider, J. S. Dornelles, L. B. Gomes, N. R. Marcilio and P. J. Melo, *Cleaner Eng. Technol.*, 2021, **4**, 100201.
10 A. Á. B. Maia, R. N. Dias, R. S. Angélica and R. F. Neves, *J. Mater. Res. Technol.*, 2019, **8**, 2924–2929.
11 S. K. Kirdeciler and B. Akata, *Adv. Powder Technol.*, 2020, **31**, 4336–4343.
12 M. Foroughi, A. Salem and S. Salem, *Mater. Chem. Phys.*, 2021, **258**, 123892.
13 S. O. Otieno, F. O. Kengara, J. C. Kemmegne-Mbouguen, H. W. Langmi, C. B. Kowenje and R. Mokaya, *Microporous Mesoporous Mater.*, 2019, **290**, 109668.
14 S. Otieno, C. Kowenje, F. Kengara and R. Mokaya, *Mater. Adv.*, 2021, **2**, 5997–6010.
15 S. Otieno, F. Kengara, C. Kowenje and R. Mokaya, *RSC Adv.*, 2022, **12**, 22792–22805.
16 S. Alraddadi and H. Assaedi, *J. King Saud Univ., Sci.*, 2020, **32**, 2969–2975.
17 M. F. Serra, M. S. Conconi, G. Suarez, E. F. Aglietti and N. M. Rendtorff, *Ceram. Int.*, 2015, **41**, 6169–6177.
18 P. N. Lemougna, U. F. Chinje Melo, M.-P. Delplancke and H. Rahier, *Ceram. Int.*, 2014, **40**, 811–820.
19 C. Leonelli, E. Kamseu, D. N. Boccaccini, U. C. Melo, A. Rizzuti, N. Billong and P. Miselli, *Adv. Appl. Ceram.*, 2007, **106**, 135–141.
20 J. Rosales, M. Rosales, J. L. Díaz-López, F. Agrela and M. Cabrera, *Materials*, 2022, **15**, 6305.
21 S. Tome, D. T. Hermann, V. O. Shikuku and S. Otieno, *Ceram. Int.*, 2021, **47**, 20965–20973.

22 C. A. Rios, C. D. Williams and M. J. Maple, *Bistua*, 2007, **5**, 15–26.

23 C. A. Ríos, C. D. Williams and M. A. Fullen, *Appl. Clay Sci.*, 2009, **42**, 446–454.

24 L. Heller-Kallai and I. Lapides, *Appl. Clay Sci.*, 2007, **35**, 99–107.

25 C. A. Ríos, C. D. Williams and O. M. Castellanos, *Ing. Compet.*, 2012, **14**, 125–137.

26 C. Baerlocher and L. B. McCusker, *Database of Zeolite Structures*, 2017, Access Date 03 December 2022. **http://www.iza-structure.org/databases**.

27 M. Singh, S. Vinodh Kumar, S. A. Waghmare and P. D. Sabale, *Constr. Build. Mater.*, 2016, **112**, 386–397.

28 S. A. Kamba, M. Ismail, T. A. Tengku Ibrahim and Z. A. B. Zakaria, *J. Nanomater.*, 2013, **2013**, 398357.

29 J. D. Rodriguez-Blanco, S. Shaw and L. G. Benning, *Nanoscale*, 2011, **3**, 265–271.

30 F. Munawaroh, L. K. Muharrami, Triwikantoro and Z. Arifin, *KnE Eng.*, 2019, **4**, 98–104.

31 W. Mozgawa, W. Jastrzębski and M. Handke, *J. Mol. Struct.*, 2005, **744–747**, 663–670.

32 M. Esaifan, L. N. Warr, G. Grathoff, T. Meyer, M.-T. Schafmeister, A. Kruth and H. Testrich, *Minerals*, 2019, **9**, 484.

33 M. K. Naskar, D. Kundu and M. Chatterjee, *Mater. Lett.*, 2011, **65**, 3408–3410.

34 R. Belaabed, S. Elabed, A. Addaou, A. Laajab, M. A. Rodríguez and A. Lahsini, *Bol. Soc. Esp. Ceram. Vidrio*, 2016, **55**, 152–158.

35 H. Tounsi, S. Mseddi and S. Djemel, *Phys. Proc.*, 2009, **2**, 1065–1074.

36 J. Zou, C. Guo, C. Wei, F. Li and Y. Jiang, *Mater. Trans.*, 2016, **57**, 726–731.

37 P. Sharma, J.-S. Song, M. Han and C.-H. Cho, *Sci. Rep.*, 2016, **6**, 22734.

38 M. Thommes, K. Kaneko, A. V. Neimark, J. P. Olivier, F. Rodriguez-Reinoso, J. Rouquerol and K. S. W. Sing, *Pure Appl. Chem.*, 2015, **87**, 1051–1069.

39 S. Shirani Lapari, Z. Ramli and S. Triwahyono, *J. Chem.*, 2015, **2015**, 272613.